H_2O to DMSO $\Delta H°_{tr} \approx 1$ kcal·mol^{-1} (Parker[23]) leads to $\Delta H°_{sol}(F^-) \approx -102$ kcal·mol^{-1} in DMSO.

The $\Delta H_{sol}(C_6F_6) = -8$ kcal·mol^{-1} is based on the vaporization enthalpy of C_6F_6, $\Delta H°_{vap} = 8$ kcal·mol^{-1},[24] and the near-zero enthalpy of mixing of liquid C_6F_6 and DMSO.[25]

(b) Change of Solvation Energy of F^- in DMSO on Displacement of One Inner-Shell DMSO Molecule with C_6F_6. A rough value can be obtained by estimating first the solvation energy of $F^-(DMSO)_4$ in DMSO. The radius of $F^-(DMSO)_4$ was estimated as 5.5 Å (see Table IV in Magnera[8]). This radius then was used to obtain the solvation energy differences between Cl^- and $F^-(DMSO)_4$ in DMSO, via the same type of extrapolation in Figure 8 (Magnera[8]) as in part a. This difference was found to be 42 kcal·mol^{-1}. Since $\Delta H_{sol}(Cl^-) = -80.3$ kcal·mol^{-1} in DMSO, see part a, the $\Delta H_{sol}(F^-(DMSO)_4) \approx -38$ kcal·mol^{-1}. Since $-\Delta H_{sol}(F^-) = 102$ kcal·mol^{-1}, see part a, the contribution of the inner shell to the solvation can be taken as $102 - 38 = 54$ kcal·mol^{-1}, and replacing one of the DMSO molecules from the inner shell of F^- with the very inefficient C_6F_6 should lead to $^1/_4$ loss of inner-shell solvation, i.e., ~ 16 kcal·mol^{-1}. Considering that this is only a rough estimate, the actual energy increase due to desolvation could easily surpass 20 kcal·mol^{-1}.

(c) Solvation Energy of $C_6F_6^{\bullet-}$. The polarographic half-wave reduction potential of C_6F_6 in dimethylformamide (DMF) has been determined as $\epsilon_{1/2} = -2.1 \pm 0.1$ V versus the saturated calomel electrode (SCE). This value when substituted into eq 11, together with the known electron attachment free energy of

$$\Delta G°_{sol}(B^-) - \Delta G°_{sol}(B) = -108 \text{ (kcal·mol}^{-1}) - 23.06\epsilon_{1/2}(B) \text{ (V)} - \Delta G°_a(B) \quad (11)$$

$B = C_6F_6$, $\Delta G°_a(B) = -14.8$ kcal·mol^{-1},[12] leads to

$$\Delta\Delta G°(C_6F_6^{\bullet-}) = \Delta G°_{sol}(C_6F_6^{\bullet-}) - \Delta G°_{sol}(C_6F_6) = -45 \text{ kcal·mol}^{-1} \text{ in DMF} \quad (12)$$

For the origin of eq 11 see Heinis.[26] The numerical constant −108 kcal·mol^{-1} is based on the single ion hydration energy of Cl^- due to Randles and is thus consistent with the thermochemistry used in parts a and b of the Appendix.

The $\Delta\Delta G°(C_6F_6^{\bullet-}) = -45$ kcal·mol^{-1} is close to the corresponding values for 1,4-dinitrobenzene, $\Delta\Delta G° \approx -48$ kcal·mol^{-1},[27] and tetrafluorobenzoquinone, $\Delta\Delta G° \approx -48$ kcal·mol^{-1}.[26] These three radical anions are expected to be strongly charge delocalized. The available $\Delta\Delta S° = -5$ cal·K^{-1}·mol^{-1} (Parker[27]) for the dinitrobenzene is assumed to be valid also for C_6F_6. This assumption leads to $\Delta\Delta H°(C_6F_6^{\bullet-}) = -46.5$ kcal·mol^{-1} in DMF.

For strongly delocalized anions the values in DMF and DMSO should be close. Taking $\Delta H_{sol}(C_6F_6) = -8$ kcal·mol^{-1} in DMSO (see part a, Appendix), one obtains a rough estimate for $\Delta H_{sol}(C_6F_6^{\bullet-}) \approx -54.5$ kcal·mol^{-1} in DMSO.

Registry No. F, 16984-48-8; C_6F_6, 392-56-3; C_6HF_5, 363-72-4; $C_6F_5CF_3$, 434-64-0; $C_6F_5OCH_3$, 389-40-2; C_6F_5CN, 773-82-0; $C_6F_5NO_2$, 880-78-4; perfluorobenzene radical anion, 37551-90-9.

(23) Parker, V. B. *Thermal Properties of Aqueous Uni-univalent electrolytes*; National Bureau of Standards: Washington, D.C., 1965; NSRDS-NBS[2]. Wu, Y. C.; Friedman, H. L. *J. Phys. Chem.* **1966**, *70*, 501, 2020. Krishnan, C. V.; Friedman, H. L. *Ibid.* **1969**, *73*, 3934; **1970**, *74*, 2356; **1971**, *75*, 388 and 3606. Abraham, M. H. *J. Chem. Soc., Faraday Trans. I* **1973**, *69*, 1375.

(24) Cox, J. D.; Gundry, H. A.; Harrop, D.; Head, A. J. *J. Chem. Thermodyn.* **1969**, *1*, 77.

(25) Mattingley, B. I.; Handa, Y. P.; Fenby, D. V. *J. Chem. Thermodyn.* **1975**, *7*, 169.

(26) Heinis, T.; Chowdhury, S.; Scott, S. L.; Kebarle, P. *J. Am. Chem. Soc.*, in press.

(27) Svaan, M.; Parker, V. D. *Acta Chem. Scand.* **1982**, *B36*, 357.

Growth of Silver Halides from the Molecule to the Crystal. A Pulse Radiolysis Study

K. H. Schmidt, R. Patel,† and D. Meisel*

Contribution from the Chemistry Division, Argonne National Laboratory, Argonne, Illinois 60439. *Received January 14, 1988*

Abstract: Halide ions were produced in situ by pulse radiolysis, via electron transfer to dihalomethanes from solvated electrons or hydrogen atoms, and were then used to generate silver halide molecules and larger aggregates. This evolution of silver halide aggregates was studied for the case of silver iodide on the time scale of 10^{-6}–10^2 s. Conductivity detection allows determination of the rate of formation of the first AgI molecule. Spectrophotometric detection of the growth of the particles from the stage of the molecular species to colloidal particles of bulk electronic properties is then possible. When the aggregates thus formed approach sizes of ca. 50 Å, their detection by light scattering provides an independent method of size determination. In the region where such measurements are possible, the sizes determined by light scattering agree with sizes calculated assuming confinement of excitons in small particles and their electron-hole coulomb screening. A similar approach is suggested for growth studies of other insoluble materials.

The growth of silver halide particles has been a subject of many studies in conjunction with their application in photographic processes.[1] The growth mechanism is particularly important in such processes since the sensitivity of the photographic material depends on its grain size as well as crystal structure. Often those studies involve electron microscopic and electron diffraction size and structure determinations and correlations with spectroscopic properties of the growing crystallites.[2-4] Such measurements, while providing a wealth of information, are naturally limited to events occuring at relatively long times after initiation of the growth process, beyond the nucleation stage. More recently Tanaka and Iwaski applied the stopped-flow technique to study

† Permanent address: Department of Chemistry, Clarkson College of Technology, Potsdam, NY 13676.

(1) James, T. H. *The Theory of the Photographic Process*; Macmillan: New York, 1977.

(2) Klein, E.; Moisar, E. *Ber. Bunsen-Ges. Phys. Chem.* **1963**, *67*, 349, 356, 949.

(3) (a) Berry, C. R.; Skillman, D. C. *J. Appl. Phys.* **1962**, *33*, 1900. (b) *Ibid. J. Phys. Chem.* **1963**, *67*, 1827. (c) *Ibid. J. Phys. Chem.* **1964**, *68*, 1138.

(4) (a) Saijo, H.; Iwasaki, M.; Tanaka, T.; Matsubara, T. *Photogr. Sci. Eng.* **1982**, *26*, 92. (b) Tanaka, T.; Saijo, H.; Matsubara, T. *J. Photogr. Sci.* **1979**, *27*, 60.

0002-7863/88/1510-4882$01.50/0

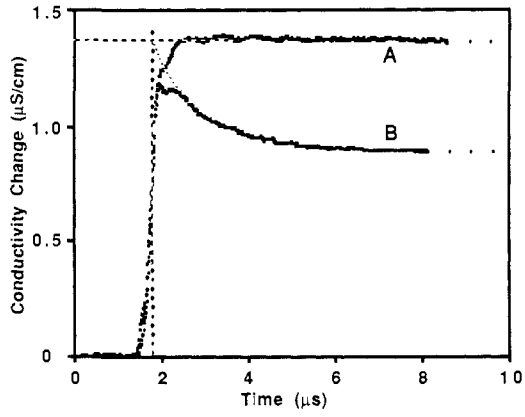

Figure 1. Production of 5×10^{-6} M iodide ions as detected by conductivity in the absence of silver ions (A) and their reaction with silver ions in the presence of 1×10^{-4} M Ag^+ (B).

the growth of silver bromide extending the time resolution to the millisecond range.[5] In their study they were able to identify three stages in the growth process: formation of complexes, nucleation, and ripening. The first step was complete within the time resolution of the technique while for the slower steps analysis was hampered by the lack of independent size determinations. In the present paper we offer a method for the study of the growth of silver halides where time resolution poses no technical limitation. It is the difficulty of identifying the various species that ultimately limits complete understanding of the evolutionary process. The technique utilizes pulse radiolysis to create halide ions within the nanosecond or microsecond time domain in solutions containing a soluble silver salt at concentrations that will cause the solubility of the silver halide to be exceeded. A combination of conductivity detection, spectrophotometric detection, and light-scattering techniques allows us to follow the growth of the particles from the stage of formation of molecular species to fully developed crystallites possessing bulk properties. The following provides preliminary results on the silver iodide system and indicates the capabilities of the technique.

Experimental Section

The pulse radiolysis technique and the conductivity and streak camera detection systems have been described elsewhere.[6] For light-scattering measurements a 5-mW Hughes (Model 3225 H-PC) He–Ne laser was used. Transmission electron microscopy and in situ elemental analysis by energy dispersive X-ray spectroscopy of the particles deposited on carbon-coated copper grids were carried out on a Philips EM 420 instrument. All solutions contained 0.5 M *tert*-butyl alcohol to scavenge OH radicals, 1×10^{-4} M Ag^+ as the sulfate salt, and 1×10^{-4} M $HClO_4$ and were Ar saturated.

Results and Discussion

Iodide ions in concentrations of $(0.05–5.0) \times 10^{-4}$ M were produced by dissociative electron transfer to diiodomethane ($0.1–1.0 \times 10^{-3}$ M) using electron pulses of widths between 4 ns and 3 μs depending on the amount of iodide to be created. The dihalomethane, rather than the monohalomethane, was chosen in order to minimize thermal reaction with the silver ions present in the solution. Two radicals are simultaneously produced in the system, the methyl iodide radical (reaction 1) and the β-alcohol

$$e_{aq}^- (H) + CH_2I_2 \rightarrow CH_2I + I^- (+H^+) \qquad (1)$$

radical from *tert*-butyl alcohol. Neither seems to have any effect on the growth of the silver halide aggregates. The amplitude of the conductivity signals in the presence or absence of Ag^+ indicates quantitative conversion of e_{aq}^- and H atoms to iodide ions and the formation of an equivalent amount of H^+ (directly from the radiolysis of water to balance e_{aq}^- and through the reaction of H

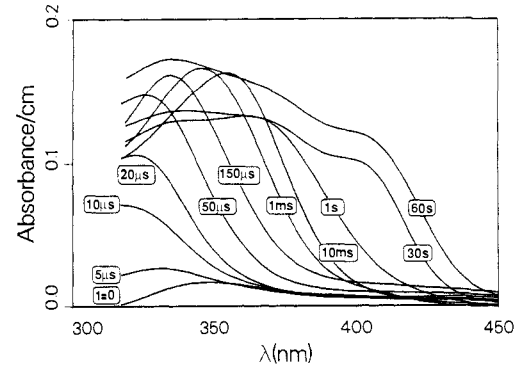

Figure 2. Spectral evolution of AgI crystallites from the molecular level to the bulk material. $[AgI]_{total} = 6.5 \times 10^{-5}$ M. Original solution contained 5×10^{-5} M Ag_2SO_4; 0.5 M *tert*-butyl alcohol at pH 4.

atoms according to reaction 1) with a yield of 3.3 iodide ions/100 eV of absorbed radiation energy. Under the experimental conditions described here the formation of iodide is complete within the pulse. The yield and rate of formation of silver iodide molecules were detected as a decrease in the conductivity signal as can be seen in Figure 1. The forward rate constant for reaction 2 was determined from these experiments to be 8.1×10^9 M^{-1} s^{-1}, i.e. practically diffusion controlled. The amplitude of the decrease in the signal in Figure 1 corresponds within experimental error to complete conversion of all the iodide produced by the pulse to silver iodide (using $\lambda_{Ag^+} = 61.9$; $\lambda_{I^-} = 76.8$ cm^2 S mol^{-1}). Complete conversion is indeed expected for these experiments from log $K_2 = 6.58$.[7] In addition, some formation of complexes such as $(Ag_nI)^{(n-1)+}$ or $(AgI_n)^{(n-1)-}$ may occur depending on which ion is present in excess in these experiments. The formation of higher silver iodide complexes, however, would only have a small effect on the conductivity signals.

$$I^- + Ag^+ \rightarrow AgI \qquad (2)$$

Spectral evolution of the silver iodide was monitored by our streak camera system over a time period extending to many seconds. Some results of these experiments are shown in Figure 2. To minimize photochemical reactions of the growing crystallites, each solution was exposed to the analytical light only for a period of ca. 10 ms. The time-resolving capability of the streak system was utilized only for time scales ≤200 μs while, for longer time scales, 10-μs snapshots of the spectrum where taken at various times after the pulse, each on a fresh solution. The spectrum taken after 60 s (Figure 2) leaves little doubt as to the identity of the final product. It is similar to the well-known spectrum of colloidal AgI and was also reproduced by mixing of silver and iodide salts and rapid measuring of the spectrum on a spectrophotometer. Furthermore, irradiated solutions that were rapidly (within minutes) deposited on electron microscope grids revealed particles of broad size distribution, whose electron diffraction pattern corresponds to the wurzite structure of β-AgI ($a = 4.59$ Å, $c = 7.51$ Å) and whose in situ EDS analysis showed only Ag and I lines. The spectra at times shorter than 10 μs represent the various complexes, and their identification will require more detailed studies than presently intended. At times longer than 50 μs, the integrated areas of the spectra are roughly constant. The formation of exciton bands could be clearly identified at times longer than ca. 50 ms, although a single maximum is observed in all spectra from the earliest times measured. The band at 370 nm in the spectra of AgI particles taken after 1 s or more has been previously observed and assigned to an intermediate phase.[4b] Alternatively, this band may indicate preferential aggregation to sizes of ≈25 Å (or limited growth in a particular direction) if it is assumed to be a confined W_1 (or W_2) exciton band[8] as discussed below. The other two bands of the final spectra are identified

(5) Tanaka, T.; Iwasaki, M. *J. Imaging Sci.* **1985**, *29*, 86.
(6) (a) Schmidt, K. H.; Gordon, S. *Rev. Sci. Instrum.* **1979**, *50*, 1656. (b) Schmidt, K. H.; Gordon, S.; Thompson, M.; Sullivan, J. C.; Mulac, W. M. *Radiat. Phys. Chem.* **1983**, *21*, 321.
(7) *Critical Stability Constants*; Smith, R. M., Martel, A. E., Eds. Plenum: London, 1976; Vol. 4, p 122.
(8) Cardona, M. *Phys. Rev.* **1963**, *129*, 69.

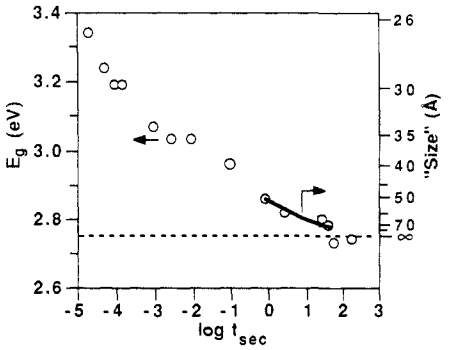

Figure 3. Optical absorption threshold, E_g, of growing AgI agglomerates as a function of time (circles). Dashed line indicates value for bulk material. The scale on the right-hand side axis is particle size, L, calculated from E_g with eq 3; the solid curve shows the average size determined from light-scattering measurements.

as the W_1 and W_3 exciton bands.[8]

Due to difficulties in determining the exact positions of the exciton bands of the growing crystallites, we prefer to report the shift of the threshold absorption, labeled E_g, to lower energies with time. These shifts were determined from the intercepts of $(\alpha h\nu)^{1/2}$ vs $h\nu$ plots (where α is the absorption coefficient in reciprocal centimeters) for each of the spectra shown in Figure 2. The shift of the absorption onset to lower energies as the particles grow is shown in Figure 3 (circles). These results are analyzed following Brus' formulation for the size dependent exciton absorption in confined dimensions.[9] Brus and co-workers have already suggested that this formulation can predict the shift for small AgI particles.[10] To account for the anisotropy of the reduced exciton effective masses, we use the modification for an anisotropic particle.[11] However, since we are able to determine only particle volumes from light-scattering measurements (see below), we assume a cubic particle of volume L^3. We also rewrite the small Coulomb screening term, derived for spherical particles, $1.8e^2/\epsilon R$, where R is the particle radius and $\epsilon = 4.9$ is the optical dielectric constant, in terms of the dimension L of a cube of the same volume. This approximation leads to eq 3 where $\mu_{x,y} = 0.18m_0$ and $\mu_z =$

$$\Delta E_g = \frac{h^2}{8}\left(\frac{1}{\mu_x} + \frac{1}{\mu_y} + \frac{1}{\mu_z}\right)\frac{1}{L^2} - \frac{2.9e^2}{\epsilon L} \qquad (3)$$

$0.28m_0$ are the reduced exciton effective masses perpendicular and parallel to the c axis, respectively.[12] When eq 3 is used, the sizes, L, corresponding to various E_g values were calculated and plotted in Figure 3 as the right-hand ordinate scale so that the two ordinate scales are equivalent.

An independent estimate of the volume-weighted average size was obtained from light-scattering measurements. Calibration and size calculations for these experiments follow the method of Hsu, Patel, and Matjevic.[13] The intensity of the scattered light is proportional to the product of the total particles volume multiplied by the volume of each particle (i.e. to nv^2 where n is the particles concentration and v is the volume of a particle). Since all our light-scattering experiments are in the Raleigh scattering regime, the scattering intensity is independent of the particle shape. From the dose (total iodide produced) and the density of silver iodide ($\delta = 6.01$ g/cm^3), we calculate the total volume of AgI and thus obtain the volume of the each particle from the scattering intensity. Sensitivity of the present system limits these measurements to $L > 50$ Å. Results from the light-scattering experiments are plotted in Figure 3 as the solid curve. The size was again calculated as the dimension $L = v^{1/3}$ to be compatible with the size determined from the absorption threshold. In the accessible range the measured sizes and those calculated according to eq 3 agree quite well. However, this excitonic model has to fail if extended beyond the limit of its approximation, when bulk effective masses and the dielectric constant are no longer relevant. This is the situation at the short times shown in Figure 3. Thus, for example, when E_g in Figure 3 is 3.3 eV (after 20 μs), eq 3 will yield particles of ca. 32 Å in diameter. Simple diffusion-limited calculations show that at these times no more than two to three AgI molecules could have aggregated. Clearly, this range is still at the molecular level regime.

Some qualitative observation on the growth process may be mentioned at this time. Early experiments indicate that at least in the slow time domain (longer than 1 s) the growth indeed follows an Ostwald ripening mechanism. In the size regime where light-scattering measurements are feasible, the observed rate of growth is faster for the more soluble halide (i.e., in the order chloride > bromide > iodide). We point out that the same method can be used to study other sparingly soluble salts as well. Production of sulfide ions from mercaptans by the same technique is presently utilized to study the growth of CdS in our laboratory.

Acknowledgment. We are grateful to the ANL linac team for the dedicated operation of the accelerator and to G. Mills and L. Zongguan for electron microscopy results. Work was performed under the auspices of the Office of Basic Energy Sciences, Division of Chemical Science, U.S. DOE under Contract No. W-31-109-ENG-38.

Registry No. CH_2I_2, 75-11-6; I_2, 20461-54-5; H_2O, 7732-18-5; AgI, 7783-96-2; Ag^+, 14701-21-4.

(9) Brus, L. E. *J. Phys. Chem.* **1986**, *90*, 2555; *J. Chem. Phys.* **1984**, *80*, 4403.
(10) Rosseti, R.; Hull, R.; Gibson, J. M.; Brus, L. E. *J. Chem. Phys.* **1985**, *83*, 1406.
(11) (a) Brus, L. E. *J. Chem. Phys.* **1983**, *79*, 5566. (b) Sandroff, C. J.; Hwang, D. M.; Chung, W. M. *Phys. Rev. B: Condens. Matter* **1986**, *33*, 5953.
(12) Solid-state parameters were taken from: *Landolt-Bornstein, New Series*; Springer-Verlag: Berlin, 1982; Vol. 17b, pp 297–301.
(13) Hsu, W. P.; Patel, R. C.; Matjevic, E. *Appl. Spectrosc.* **1987**, *41*, 402.